JOURNAL OF MATERIALS SCIENCE 29 (1994) 1295–1301

Fabrication of glass-capsuled CdTe microcrystals using laser evaporation and plasma chemical vapour deposition method

K. TSUNETOMO, S. OHTSUKA, T. KOYAMA, S. TANAKA
Tsukuba Research Laboratory, Nippon Sheet Glass Co. Ltd, 5–4 Tokodai, Tsukuba, Ibaraki 300–26 Japan

CdTe microcrystals encapsulated in a silica glass layer were successfully fabricated. Spherical CdTe microcrystals were prepared by laser evaporation of a CdTe target in an argon gas atmosphere. The ensuing microcrystals plus argon gas passed through a tetramethoxysilane (TMOS) + O_2 plasma in which they were encapsulated in an amorphous layer, 2–2.5 nm thick. Characteristic X-rays from the surface layer were measured using an energy dispersive X-ray spectrometer equipped in a high-resolution transmission electron microscope. Measurements indicated that the glass layer consisted of silicon and oxygen, with no cadmium or tellurium included. The CdTe microcrystals fabricated with our laser evaporation system showed two specific kinds of particle: small particles (below 10 nm) and large ones (over 100 nm). Using precise electron-beam diffraction testing, we concluded that the large microcrystal is a single crystal with a hexagonal structure. The deposition rates and infrared transmission of silica glass prepared by TMOS or tetraethoxysilane plasma-enhanced chemical vapour deposition are also discussed. The highest deposition rate, 30 nm s^{-1}, of silica glass can be achieved in the centre of the plasma when the input r.f. power is 150 W.

1. Introduction

Numerous studies on semiconducting microcrystals, such as CdS, CdSe, CdTe, Si, Ge and CuCl, have been carried out to investigate zero-dimensional confinement effects on electron–hole systems [1–9]. Such microcrystals also attract interest because of their large optical non-linearity and fast relaxation time [10–12]. ($\chi^{(3)}$ is defined by $\boldsymbol{p}^{(3)} = \varepsilon_0\chi^{(3)}\boldsymbol{E}^{(3)}$ where $\boldsymbol{p}^{(3)}$ is third order nonlinear polarization and E is electric field.) For application to optical non-linear devices, a larger optical non-linear susceptibility, $\chi^{(3)}$, is required. The best-known enhancement of optical non-linearity is achieved with the use of the exciton confinement effect. Great enhancement of the optical non-linearity of excitons was theoretically predicted by Hanamura [13], and has been sequentially examined by several researchers working with CuCl microcrystallites [7–9]. Until recently, however, there seemed to be little promise for such enhancement in other semiconducting microcrystallites such as II–VI or III–V type because of their relatively large Bohr radius, in which the electrons and holes are individually confined.

Recently, Birnboim and co-workers [14, 15] theoretically predicted an enhancement effect near the resonance of the surface plasmon. For this case, the microcrystallites have to be coated with a metal layer. Although the effect is thought to be applicable for any microcrystallite, it has not lent itself to examination because of the lack of fabrication techniques for metal-capsuled microcrystals. One possible technique is precipitation of metal on to the surface of semiconducting colloids to apply a coating in solution. Unfortunately, this method applies only to those few microcrystallites which are easily formed in solution.

We previously reported a new fabrication technique for microcrystals, the laser evaporation (LE) method [16–18], in which the source of the microcrystal was instantaneously evaporated by high-power pulsed laser irradiation and the microcrystals themselves were formed through a quenching process of the evaporated atoms with inert gas. The LE method lends itself to application for many kinds of microcrystals such as GaAs which cannot otherwise be obtained. The microcrystalline size can be controlled by changing the pressure of the inert gas and variation of the laser power. Another interesting feature of the method is that the microcrystals are formed in the gaseous state and so can be easily transferred with the inert gas. We had expected that the microcrystals could be encapsulated by transferring them through a metal alkoxide plasma.

Before fabricating the metal-capsuled microcrystallites, we tried fabricating glass-capsuled microcrystals using silicon alkoxide because the chemical vapour deposition (CVD) process for this system is well established in very large scale integration (VLSI) technology. In this paper, we report a new fabrication technique for glass-capsuled microcrystals. The source of the glass layer is a metal alkoxide, tetramethoxysilane (TMOS) or tetraethoxysilane (TEOS). We expect that our technique can be also applied to the fabrication of

0022–2461 © *1994 Chapman & Hall*

metal-capsuled microcrystals by substituting the source of the gas from silicon alkoxide to some metal organic substance.

Our interest was focused on the fabrication of metal-capsuled microcrystals. However, glass-capsuled microcrystals themselves have possibilities for other applications. For example, a glass layer on the surface of microcrystals would protect them from moisture, and/or reduce the activity of the microcrystals. A glass layer could also act as a barrier to avoid direct connection between microcrystals. Our new approach reported here shows promise for these applications.

2. Experimental procedure

Fig. 1 shows a schematic drawing of the apparatus used to fabricate the glass-capsuled CdTe microcrystals. The apparatus consists of three chambers; the evaporation chamber (EC), reaction chamber (RC) and collection chamber (CC). The CdTe microcrystals were fabricated in the EC by irradiation of a high-power pulsed laser on to a CdTe polycrystalline wafer under an argon pressure of ~ 1 torr. The excitation laser beam was a frequency-doubled output ($\lambda = 532$ nm) of a Q-switched Nd:YAG laser of which the maximum power is 200 mJ/pulse, pulse duration was about 10 ns and the frequency of incidence was 10 Hz. The energy density of the laser beam at the surface of the target was 6 J cm^{-2}. The CdTe wafer had 99.99% purity.

The RC was a fused-silica tube, 5 cm diameter, and a copper coil was fixed around it. Silicon alkoxide vapour evaporated in a vessel floated in a heat bath was introduced into the chamber with oxygen gas. The flow rates of silicon alkoxide and oxygen were controlled individually from 0–200 standard $cm^3 min^{-1}$. On supplying an r.f. voltage to the coil, a plasma formed at the centre of the RC. The input r.f. power was 10–150 W, and its frequency was 13.56 MHz.

The microcrystals fabricated in the EC were transferred to the RC through a transfer pipe, 0.5 cm diameter, with argon gas. The microcrystals were then collected on to a microgrid at the end of RC. We used a collection vessel made of stainless steel, 2.5 cm diameter and 15 cm long, to avoid excessive glass deposition on the collected microcrystals.

We used a JEOL JEM-200CX electron microscope for the transmission electron microscope (TEM) measurements, and a Hitachi HF-2000 for the energy-dispersive X-ray spectrometer (EDX) measurements. The electron probe size for EDX measurement was ~ 1 nm.

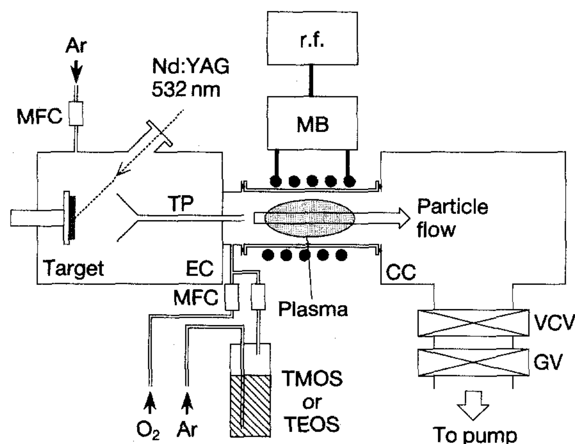

Figure 1 Schematic drawing of the apparatus used in our experiments. EC, evaporation chamber; CC, collection chamber; TP, transfer pipe; MB, matching box; r.f., radio frequency high-voltage source; VCV, variable conduction valve; GV, gate valve; MFC, mass flow controller.

3. Results

3.1. CdTe microcrystals

To begin with, we evaluated the microcrystalline size introduced into the RC. Some microgrids were placed in the RC and the collection vessel, see schematic drawing shown in Fig. 2. The gas pressure of the EC and RC were controlled to be 1 and 0.1 torr, respectively, by introducing argon into the EC and Ar + O_2 into the RC. This is almost the same for the conditions for capsule formation, except for substitution of silicon alkoxide gas by argon gas.

Transmission electron micrographs of microcrystals collected at each position are shown in Fig. 2 a–d which correspond to the positions A–D of the microgrids. At position A, all kinds of microcrystals can be seen to have collected in the RC. The photograph reveals small particles smaller than 10 nm and a few large microcrystals larger than 100 nm. Both types of crystal are single crystal. The reason for this will be discussed later.

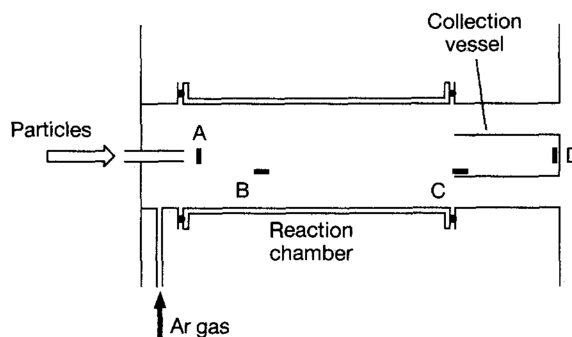

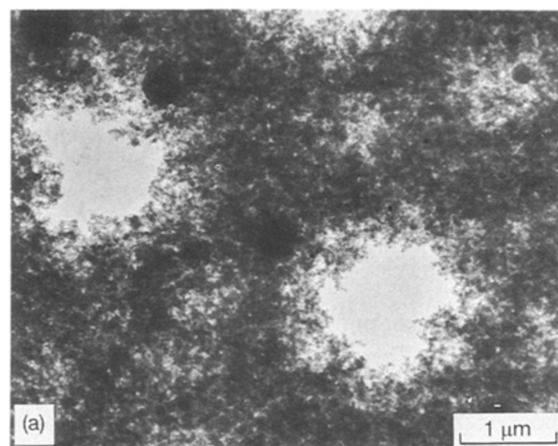

Figure 2 Transmission electron micrographs of collected microcrystals: (a)–(d) are taken at positions A–D of the microgrids as shown in the diagram; (b–d) were collected at the same time.

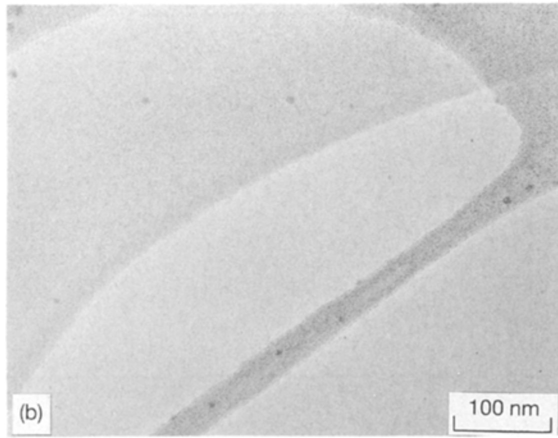

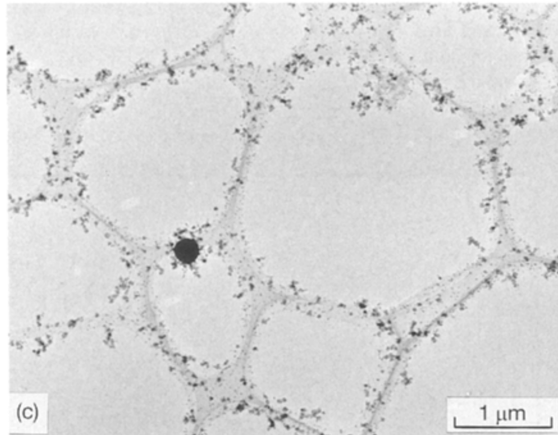

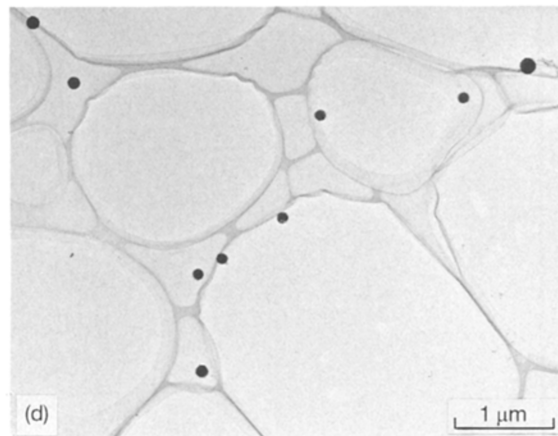

Figure 2 (Continued)

Some of the introduced microcrystals diffused towards the wall of the silica tube while the remaining microcrystals reached the bottom of the collection vessel. Fig. 2b and c show particles diffused from the centre of the particle stream, and Fig. 2d shows the remaining microcrystals. From these micrographs, we can deduce the flow and diffusion of the particles in the RC.

In the narrow tube, the velocity of particles transferred with gas is almost the same as that of the gas flow, and does not depend on a particle volume. In our case, the total amount of argon gas introduced into the EC can be evaluated through the narrow pipe. Thus, the velocity, v, of argon gas at the end of the pipe is calculated by

$$v = Q/p\pi R^2 \quad (1)$$

where Q, p and R are the gas flow rate, gas pressure and radius of the pipe, respectively. In our experiments, Q, p and R are 25 standard $cm^3 min^{-1}$ (= 317.5 torr $cm^3 s^{-1}$), 0.1 torr and 0.25 cm. Thus, the velocity of argon gas at the exit of transfer pipe is about 1.62×10^4 cm s^{-1}. In the RC, the gas velocity remarkably decreases and the particles diffuse towards the wall of RC. In this process, the microcrystals are dispersed by collision with the gas molecules. Therefore, the small particles more easily change their direction than the large particles.

In the collection vessel, the particles suddenly lose their speed. All of the small particles dispersed at the entrance of the tube and only a few of the large (heavy) particles reach the bottom of the collection tube.

3.2. SiO_2 glass

The fabrication of SiO_2 glass using plasma-enhanced chemical vapour deposition (PECVD) has been well studied for application to dielectric films for VLSI [19–21]. For our purpose, as a high deposition rate was required because the particles pass through the plasma in a very short time, we examined the dependence of the deposition rate of SiO_2 glass film on plasma conditions.

Fig. 3 shows the dependence of the deposition rate of r.f. power when TMOS was used. The horizontal axis is the distance from the exit of the transfer pipe. In this experiment, argon gas was not introduced from the EC. However, the effect of argon gas on the deposition rate was found previously to be quite small. The deposition rates were obtained from the step height of the film deposited on a glass slide after 10 min deposition. The centre of the plasma locates at about 6 cm from the exit of the transfer pipe. When a high r.f. power is supplied, the highest deposition rate, over 30 nm s^{-1}, is obtained at the centre of the plasma. On the other hand, under low r.f. power conditions, there is no maximum peak. This means that the confinement of the plasma is not sufficient and the plasma spreads toward the CC. Although higher r.f. power provides a higher deposition rate, the film

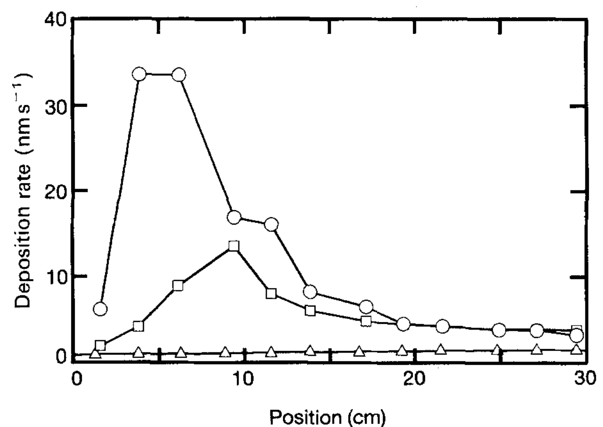

Figure 3 Dependence of deposition rate of SiO_2 glass on input power for TMOS PECVD. The horizontal axis is the distance from the exit of the transfer pipe. Oxygen flow rate = 100 standard $cm^3 min^{-1}$. Input power: (○) 150 W, (□) 100 W, (△) 50 W.

quality is not sufficient. The film prepared under an r.f. power of 150 W is transparent but light yellow. The infrared (IR) spectrum of this film indicates no residual organic substances, as shown in Fig. 4. The light-yellow colour of the film seems to be caused by some vacancies due to the lack of oxygen.

Fig. 5 shows the dependence of the deposition rate on oxygen gas flow rate for TMOS (the r.f. power is 50 W). The deposition rate increases with decreasing oxygen flow, and the highest deposition rate is obtained when the oxygen flow rate is 10 standard $cm^3 min^{-1}$. Though the film is transparent, some excessive organic substances are observed as shown in Fig. 6. Absorption peaks marked by circles correspond to $-CH_3$, $Si-CH_3$ or Si–H vibrations. They are not detected in films prepared with over 50 standard $cm^3 min^{-1}$ O_2 flow. Oxygen has an important role during the decomposition and is related to the formation of some intermediate species.

We also examined TEOS as the glass source. The tendencies in terms of the deposition rate on the plasma condition were almost the same as that for TMOS. Under the same conditions, TMOS has a larger deposition rate than in TEOS. Furthermore, by IR transmission measurement, it is recognized that film prepared using TEOS has many excesses of compounds compared to TMOS film.

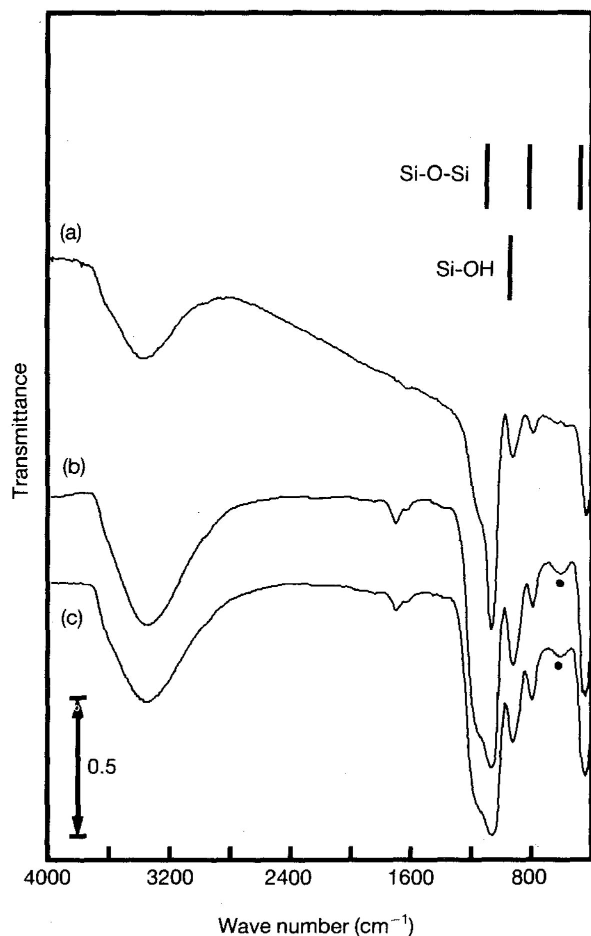

Figure 4 IR transmission spectra of SiO_2 glass prepared by TMOS PECVD under several input powers: (a) 50 W, (b) 100 W and (c) 150 W. Straight lines correspond to positions of vibrational modes of Si–O–Si and Si–OH.

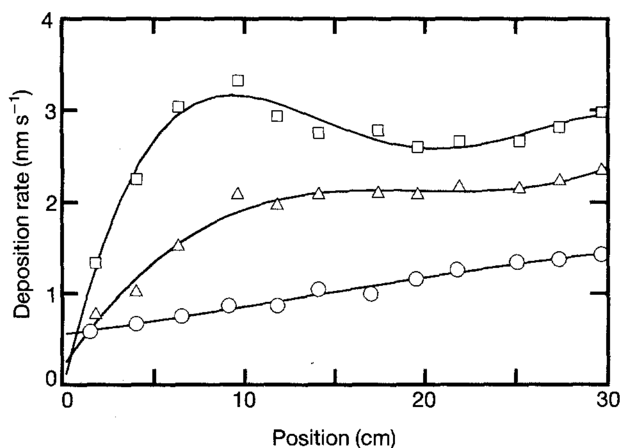

Figure 5 Dependence of deposition rate of SiO_2 glass on oxygen gas flow rate. TMOS gas flow rate was controlled to be about 200 standard $cm^3 min^{-1}$ for each film. R.f.power = 50 W. Oxygen flow rate (standard $cm^3 min^{-1}$): (□) 10, (△) 50, (○) 100.

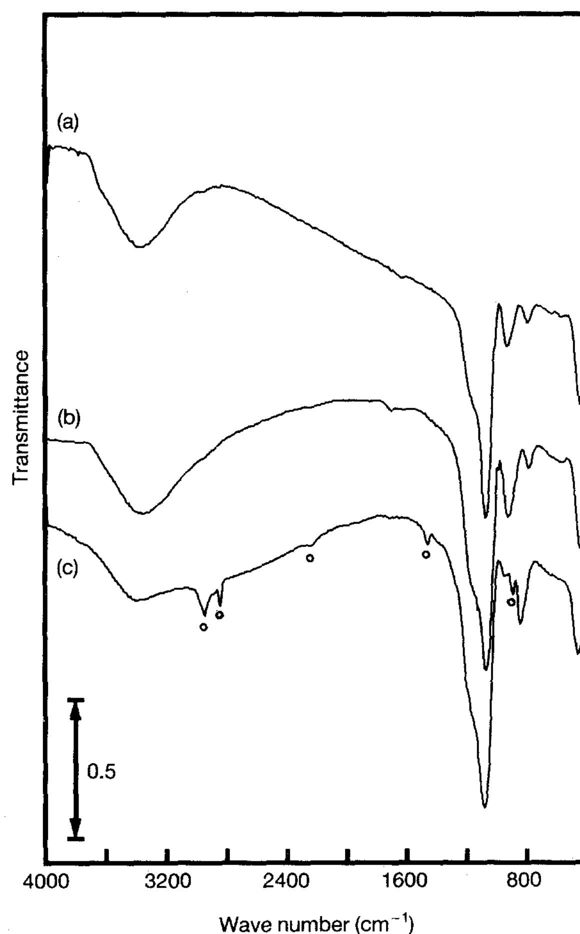

Figure 6 IR transmission spectra of SiO_2 glass prepared by TMOS PECVD under several $TMOS/O_2$ gas flow ratios: (a) 2, (b) 4, and (c) 20. Absorption peaks marked with circles correspond to $-CH_3$, $Si-CH_3$ or Si–H vibrations.

Through the above experiments, we chose to follow the plasma conditions for microcrystal encapsulation of r.f. power, 50 W, O_2 flow rate, 50 standard $cm^3 min^{-1}$ and TMOS flow rate, about 200 standard $cm^3 min^{-1}$.

As described previously, the velocity of the particles injected into the RC were calculated to be 1.62 ×

10^4 cm s^{-1}. This time, we calculated the velocity at the end of RC to be 4×10^3 cm s^{-1}. Assuming that the average velocity is 1.2×10^4 cm s^{-1} and deposition rate is constant at any location in the RC, the glass capsule thickness should be about 1.1 nm. This value is compared with the experimental values obtained, as described in the next section.

3.3. SiO_2 glass-capsuled CdTe microcrystals

Fig. 7a shows a transmission electron micrograph of a glass-capsuled CdTe microcrystal collected at the bottom of the collection vessel. Spherical crystalline CdTe can be seen. Fig. 7b is an electron-beam diffraction pattern of the CdTe microcrystal. The clear diffraction spots suggest the CdTe microcrystal is a single crystal. All of the nearest six spots are the same distance from the centre spot; the calculated plane separation is 0.398 nm, and the angles between the spots are 60°. These values agree well with those of würtzite CdTe. The largest plane separation of zinc-blende CdTe is 0.374 nm, (1 1 1) plane, and the angle between (1 1 1) planes is 70.5°. We assigned some spots to the würtzite CdTe as shown in Fig. 7b. However, as the small particles show zinc-blende structure, this suggests that these microcrystals are formed through different processes.

Fig. 8 shows a high-resolution image of the surface of a capsuled CdTe-microcrystal. The amorphous layer, 2–2.5 nm thick, can be clearly seen on the surface of the CdTe single crystal. EDX signals from the surface layer and inside a CdTe microcrystal are shown in Fig. 9. Note that the electron probe size used for this measurement is about 1 nm. Thus, we can observe a signal from only the surface layer. The surface layer consists of silicon and oxygen, and no lines corresponding to cadmium or tellurium are observed. Unfortunately, we cannot decide the Si/O ratio from this figure because the resolution near the oxygen signal is insufficient. The result of X-ray photoelectron spectroscopy (XPS) measurement on a film consisting of glass-capsuled microcrystals however, indicates that the Si/O ratio is almost 1/2. Thus, the surface layer is thought to be SiO_2 glass. Silicon and oxygen signals are also observed in Fig. 9b with strong cadmium and tellurium lines. In this case, the silicon and oxygen signals radiate from the encapsuled layer of the microcrystal at the point where the electron probe irradiates. This suggests that the microcrystal is homogeneously covered by the glass layer.

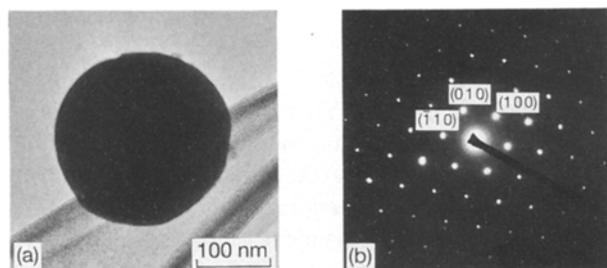

Figure 7 (a) Transmission electron micrograph of a glass-capsuled CdTe microcrystal collected at the bottom of the collection vessel and (b) the corresponding electron diffraction pattern.

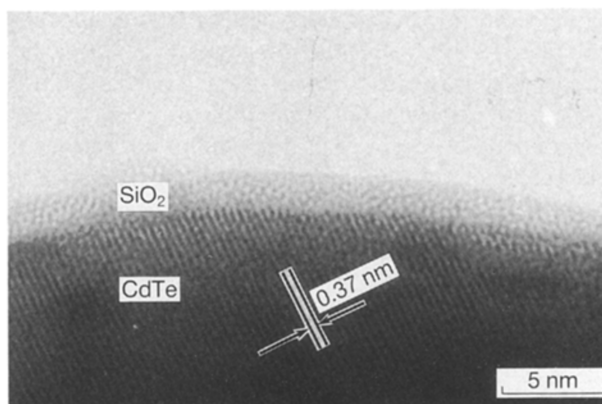

Figure 8 Magnification of the surface of a glass-capsuled microcrystal. Lines observed in the figure correlate to the (0 0 2) plane of hexagonal CdTe.

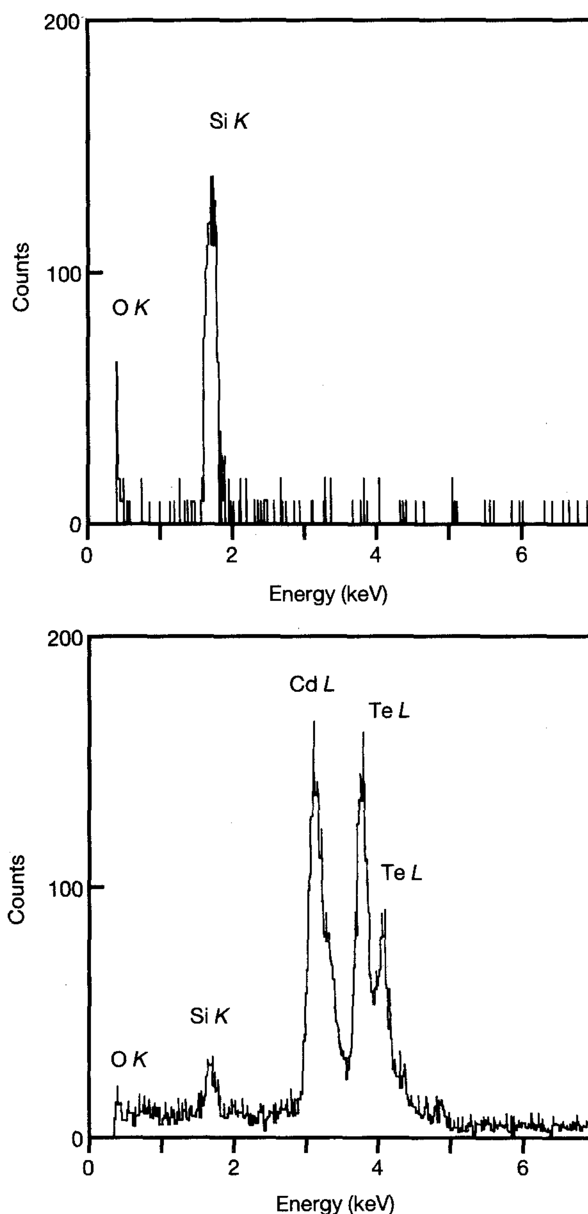

Figure 9 EDX signals from (a) the surface and (b) inside the glass-capsuled CdTe crystal shown in Fig. 8.

4. Discussion

In our method, we obtained spherical CdTe single crystals, a few hundred nanometres in diameter, and microcrystallites less than 10 nm. The absence of

middle-sized microcrystals suggests that the crystals are created in two different processes. For the large ones to form through cohesion of small particles, they would have to have a polycrystalline form. In fact, we do occasionally observe a polycrystalline particle with spherical microcrystals, but in general the shape of the polycrystal is not spherical and the microcrystals observed have many boundaries. The large spherical crystal observed at the exit of the transfer pipe is as shown in Fig. 2a. This suggests that the microcrystals are formed in the EC. In a gas evaporation process, it is generally supposed that microcrystals are created through condensation involving evaporated atoms cooling in the inert gas. Such a model would explain the formation of the small microcrystallites in our experiments. Their particle size can be controlled by changing the inert gas pressure. On the other hand, the size of the large microcrystal does not depend on the inert gas pressure. We believe the formation of a large microcrystal relates to the thermal dynamics on the surface of the CdTe target. High-power laser irradiation creates not only neutral atoms, ions, radicals and clusters, but also large droplets. Because these large droplets quench slowly, they become spherical single crystals. We are now progressing with some experiments on the particle creation process using a spectroscopic technique. The abovementioned model will be verified by these experiments.

The deposition rate and quality of the SiO_2 glass depend greatly on the plasma conditions; r.f. power, $TMOS/O_2$ flow rate, etc. We have not yet examined the reaction of TMOS or TEOS in a plasma. However, I.R. measurements reveal some information on the creation of additive organic substances and on the local structure of the glass. As shown in Figs 4 and 6, IR spectra of glasses prepared by the PECVD method to display some absorption peaks. The vibrations observed near 450, 800 and 1075 cm^{-1} are well-known Si–O–Si modes corresponding, respectively, to rocking, bending and stretching. The broad absorption near 3400 cm^{-1} and the sharp absorption near 1800 cm^{-1} relate to vibrations of H_2O, while the absorption near 900 cm^{-1} is the Si–OH vibration. We can also observe a relatively broad band near 600 cm^{-1} for films deposited under high r.f. power, marked by the closed circle in Fig. 6. This peak seems to correspond to four sited silicons [22]. Films deposited under low oxygen flow rate have excessive absorption peaks corresponding to Si–H, Si–CH_3 or –CH_3. These results indicate that the higher r.f. power causes the decomposition of TMOS, with oxygen playing an important role.

The thickness of the glass layer deposited on the CdTe microcrystals was 2–2.5 nm, i.e. 1.5 times larger than the predicted value. This may have resulted from the uncertainty of the particle speed and the variation of the deposition rate of SiO_2 in the RC. We used a collection vessel to avoid excessive deposition of SiO_2 on to the microgrid and the adhered capsule. Because the vessel narrows the path of gas flow at the end of the RC, the pressure in the RC increases. This effects an increase in the deposition rate of the SiO_2 glass in the plasma. An acceptable thickness of glass layer is thus obtained.

5. Conclusions

SiO_2 glass-capsuled CdTe microcrystals were fabricated by a low-pressure process; TMOS PECVD with the laser evaporation method. Spherical CdTe microcrystals of a few hundred nanometers were fabricated by the laser evaporation of a polycrystal CdTe target in argon gas. The microcrystals transferred to the reaction chamber in which a plasma of TMOS and O_2 were formed. They were covered by a SiO_2 glass layer 2–2.5 nm thick. EDX measurements using an electron probe beam suggest that the surface layer consists of only silicon and oxygen.

The features of our new method can be summarized as follows:

1. The laser evaporation method can be applied for a wide variety of materials such as II–VI, III–V compounds or metal particles. The PECVD method can also be applied for many materials such as oxides or nitrides by simply changing the gas source. We can choose combinations of core/shell materials, i.e. semiconductor-covered SiO_2, semiconductor/metal or metal/SiO_2. Several materials which cannot be fabricated by other methods, together with new composite particles, can be fabricated by our new method. We are now trying to fabricate metal-coated semiconductor microcrystals, and the results of these experiments will be reported in the near future.

2. The process reported in this paper is a reaction in the gaseous phase with particles transferred in a gas flow. Several possibilities exist as to techniques to grade and separate particles of the same size from the total particles produced in the gaseous state. We will apply such techniques to our new fabrication method.

3. The thickness of the capsule is limited by the particle speed and the deposition rate of silica glass. To fabricate a microcrystal with a thicker capsule, the particle speed would have to be decreased or the deposition rate increased. The gas pressure is increased to reduce the particle speed; however, the particles become dispersed by collisions with the gas, and cannot run through the plasma with ease. This contradiction becomes of more importance when smaller capsules are desired. In this sense, it is felt that another process to produce higher deposition rates in lower gas pressures would be required. We think ECR plasma deposition shows itself to be a viable method for such a purpose.

Acknowledgements

The author thank Mr T. Yoshimura, Science Technology Co. Ltd, Japan, for his cooperation in the plasma CVD experiments, and Dr A. Matsuda, Nippon Sheet Glass, for fruitful discussions. This work was performed under the management of Japan High Polymer Center as a part of the R&D Project on Basic Technologies for Future Industry supported by the New Energy and Industrial Technology Development Organization.

References

1. A. I. EKIMOV, AL. L. EFROS and A. A. ONUSHCHENKO, *Solid State Commun.* **56** (1985) 921.
2. N. F. BORRELLI, D. W. HALL, H. J. HOLLAND and D. W. SMITH, *J. Appl. Phys.* **61** (1987) 5399.
3. J. WARNOCK and D. D. AWSCHALOM, *Phys. Rev.* **B32** (1985) 5529.
4. T. ARAI, H. FUJIMURA, I. UMEZU, T. OGAWA and A. FUJII, *Jpn. J. Appl. Phys.* **28** (1989) 484.
5. S. HAYASHI, M. FUJII and K. YAMAMOTO, *ibid.* **28** (1989) L1464.
6. K. TSUNETOMO, H. NASU, H. KITAYAMA, A. KAWABUCHI, Y. OSAKA and K. TAKIYAMA, *ibid.* **28** (1989) 1928.
7. T. ITOH, Y. IWABUCHI and M. KATAOKA, *Phys. Status Solidi b* **145** (1988) 567.
8. *Idem, ibid.* **146** (1988) 531.
9. A. NAKAMURA, T. TOKIZAKI, H. AKIYAMA and T. KATAOKA, *J. Lumines.* **53** (1992) 105.
10. R. K. JAIN and R. C. LIND, *J. Opt. Soc. Am.* **73** (1983) 647.
11. S. S. YAO, C. KARAGOLEFF, A. GABLE, R. FORTENBERRY, C. T. SEATON and G. I. STEGEMAN, *Appl. Phys. Lett.* **46** (1985) 801.
12. J. YUMOTO, S. FUKUSHIMA and K. KUBODERA, *Opt. Lett.* **12** (1987) 832.
13. E. HANAMURA, *Phys. Rev.* **37** (1988) 1273.
14. M. H. BIRNBOIM and W. P. MA, in "Material Issues in Microcrystalline Semiconductors", Materials Research Society Symposium Proceedings, Vol. **164** (Materials Research Society, Pittsburg, PA, 1990) p. 277.
15. N. KALYANIWALLA, J. W. HAUS, M. H. BIRNBOIM, R. INGUVA and W. P. MA, *ibid.*, p. 283.
16. T. KOYAMA, S. OHTSUKA, H. NAGATA and S. TANAKA, *J. Cryst. Growth* **117** (1992) 156.
17. S. OHTSUKA, T. KOYAMA, K. TSUNETOMO, H. NAGATA and S. TANAKA, in "Proceedings of International Conference on Laser Advanced Materials Processing", Nagaoka, June 1992, p. 917.
18. *Idem, Appl. Phys. Lett.* **61** (1992) 2953.
19. F. S. BECKER, D. PAWLIK, H. ANZINGER and A. SPITZER, *J. Vac. Sci. Technol.* **B5** (1987) 1555.
20. A. M. NGUYEN and S. P. MURAKA, *ibid.* **B 8** (1990) 533.
21. C. P. CHANG, C. S. PAI and J. J. HSIEH, *J. Appl. Phys.* **67** (1990) 2119.
22. H. YOSHINO, K. KAMIYA and H. NASU, *J. Non-Cryst. Solids* **126** (1990) 68.

Received 2 March
and accepted 24 August 1993